Sound synthesis of Siku and closed pipe flutes

P. De La Cuadra[a], P. Magron[a], R. Auvray[b], F. Meneses[a] and B. Fabre[c]
[a]Pontificia Universidad Catolica, De Chile, Santiago, Jaime Guzman E.3300, E.3300 Santiago, Chile
[b]LAM IDA UMR 7190 Sorbonne Univ., UPMC Univ Pari, 11, rue de Lourmel, 75015 Paris, France
[c]LAM/d'Alembert, Sorbonne Universités, UPMC Univ. Paris 06, UMR CNRS 7190, 11, rue de Lourmel, 75015 Paris, France
benoit.fabre@upmc.fr

Sound synthesis by physical modeling of flute-like instruments has been developed in various contexts and development environments, from acoustical research to musical applications. The intruments that have atired most attention among researchers are recorders, organ pipes and flutes. Latin American flutes from the Andean region show some specific features that are distinctive from these instruments, both from the physical operation and from the aesthetics of the sound produced. The present study focuses on these closed pipes traditional flutes, used in open-air rites since pre-Hispanic times in Latin America. Both the power and the timbre structure of the sound are challenging for physical modeling. The resonant frequencies show a peculiar structure and the closed pipe induces a recirculation of the portion of the air flux that gets into the pipe, affecting the hydrodynamics of the jet. The high jet flux, required to play the instrument, produces a flow structure that rapidly becomes turbulent. The physics of the instrument has been modeled and simulated in a real-time platform to make it available for musical exploration.

1 Introduction

A flute-like instrument, different from those found in Europa, was a central object in some pre-hispanic cultures in South America. They were built in different materials such as stone, wood or ceramic. They have a peculiar resonator made out of two (or three) cylinders of different diameters and precise lengths. They are capable of producing a loud and vibrant sound called *sonido rajado* (literally torn sound) that was very appreciated and still is in some rural villages in South America. The most delicately crafted of these type of instruments is the antara, a set of 4 or 5 pipes built together in a piece of stone or ceramic. It was more than a musical instrument an important cultural, religious and social symbol. Throughout this article the physics of the resonator of an antara-like instrument are described and a simulation model is proposed and implemented.

2 Acoustic model of the resonator

The resonator is modeled as a closed pipe made out of two cylindrical sections with different diameters. Figure 1 shows a sketch with the geometry of the instrument and the definition of the pressure waves.

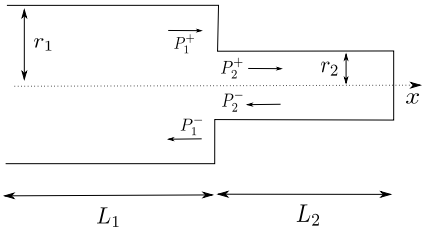

Figure 1: Complex resonator model

Plane longintudinal waves are assumed inside the resonator. D'Alembert's decomposition leads to write the wave variables as the sum of right traveling and left traveling functions.

2.1 Two-port junction

At the junction between the two sections of the resonator, physical constraints must be respected. Flow rate equality and pressure continuity leads to a relation between traveling pressure, as detailed in [1].

$$\begin{cases} P_2^+ = P_1^+ + r_k(P_1^+ - P_2^-) \\ P_1^- = P_2^- + r_k(P_1^+ - P_2^-) \end{cases} \quad with r_k = \frac{r_1^2 - r_2^2}{r_1^2 + r_2^2} \qquad (1)$$

2.2 Visco-thermal losses

Visco-thermal losses are described by a complex wave number:

$$k = i\frac{\omega}{c} + (1+i)\frac{\beta}{r}\sqrt{f} \qquad (2)$$

This wave number takes into account the phenomenon of propagation $i\frac{\omega}{c}$, dissipation $\frac{\beta}{r}\sqrt{f}$ which is the loss of energy due to the visco-thermal effect, and dispersion $i\frac{\beta}{r}\sqrt{f}$ which impacts on the resonant frequencies.

2.3 Input admittance

Blanc [2] develop a method to obtain the input admittance of the resonator:

$$Y_{in} = \frac{1 + r_k(H_2 - H_1) - H_1H_2}{1 + r_k(H_2 + H_1) + H_1H_2} \qquad (3)$$

with the transfer functions H_j of each cylinder:

$$H_j = e^{-2k_jL_j} \qquad (4)$$

To evaluate the accuracy of such a model, we have built a complex resonator prototype, measured its admittance and compared it with the proposed model.

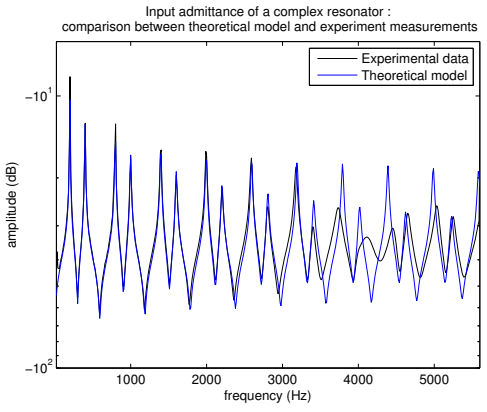

Figure 2: Comparison between the theoretical and LMA prototype complex resonator input admittance. Prototype geometry is: $L_1 = L_2 = 28cm$, $r_1 = 9mm$ and $r_2 = 5mm$

Conformingly to the work conducted in [2], we observe double admittance maxima. Globally, the theoretical model reproduces with high accuracy the measurement, especially in the low-frequency domain. We observe a significant difference around 4000 Hz, but this may be explained by a coupling between the prototype and the measurement device, whose first eigen-frequency is close to this value.

2.4 Radiation

To complete the acoustic model of the resonator, we need to take into account the radiation at the open end. We use the circular plate model. Let a be the plate radius and S its surface. The radiation impedance is given by Eq. (5)

$$Z_{rad} = Z_c(\alpha_r(ka)^2 + i\alpha_i ka) \tag{5}$$

$Z_c = \frac{\rho c}{S}$ is the characteristic admittance, α_r and α_i depends on the geometry of the equivalent screen around the plate. In the case of the antara we can set α_r to $1/4$ but we leave α_i variable to take into account different instruments size.

This expression is valid until $ka = 1$ (low-frequency domain), i.e. for frequencies below $10kHz$.

2.5 Resonant frequencies

Resonance is observed when the input impedance of the resonator is null. From Eq. (3) we obtain the resonance condition:

$$\tan(\Im(k_1)L_1)\tan(\Im(k_2)L_2) = \frac{S_1}{S_2} \tag{6}$$

This condition only depends on the imaginary part of the complex wave number. Indeed, the real part of k acts on the energy loss due to dissipation, not on the frequency peaks positions.

2.5.1 Resonant frequencies without losses

A first order approximation consists in considering propagation without any losses. In this case, the wave number is $k_1 = k_2 = ik = i\frac{\omega}{c}$. As in [2] we make the assumption $L_1 \approx L_2 \approx L$. Then we formulate the resonance condition:

$$\cos 2kL = -r_k \tag{7}$$

Eq. (7) can be solved analytically. This leads to the expression of resonant frequencies of the complex resonator without losses:

$$\widetilde{f} = f_0 \times \begin{cases} 3n + \frac{3}{2}(1 - \frac{1}{\pi}\arccos r_k) \\ \\ 3n + \frac{3}{2}(1 + \frac{1}{\pi}\arccos r_k) \end{cases} \quad n \in \mathbb{Z} with f_0 = \frac{c}{6L} \tag{8}$$

As observed on Figure 2, resonant frequencies are decomposed in two series that are "almost" harmonic. It is interesting to determine a condition to observe a perfect harmonicity of each series. Those frequencies then form a single harmonic series where one partial over three is missing. Such a condition is determined by:

$$\frac{3}{2}(1 - \frac{1}{\pi}\arccos r_k) = 1 \tag{9}$$

which solution is $r_k = 1/2$. More explicitly, this corresponds to a ratio between cylinder radius $\sqrt{3}$. We will refer to it as the lossless ratio.

2.5.2 Resonant frequencies with losses

If we take the losses into account, Eq. (6) becomes:

$$(1-\frac{S_1}{S_2})\cos((\frac{L_1}{r_1}-\frac{L_2}{r_2})\beta\sqrt{f}) = (1+\frac{S_1}{S_2})\cos(4\pi L\frac{f}{c}+(\frac{L_1}{r_1}+\frac{L_2}{r_2})\beta\sqrt{f}) \tag{10}$$

with S_1 and S_2 the sections of the cylinders. For a standard geometry and a high frequency limit of $6000Hz$, then $|(\frac{L_1}{r_1} - \frac{L_2}{r_2})\beta\sqrt{f}| \approx 0.05$. We decide then to neglect this term. The condition becomes equivalent to a second-degree polynomial in $\sqrt{f}$. The only solution physically admissible can then be approximated by:

$$f_{res} = \widetilde{f} - b\sqrt{\widetilde{f}}, b = (\frac{L_1}{r_1} + \frac{L_2}{r_2})\frac{c\beta}{4\pi L} \tag{11}$$

where $\widetilde{f}$ refers to the resonant frequencies in the lossless case. As the distance between f_{res} and $\widetilde{f}$ is not constant, it is impossible to find a condition that leads to a perfect harmonicity of the series. However, calculation shows that the lossless ratio cancels inharmonicity for the high frequencies. We examine more precisely the harmonicity condition for the first partials (low-frequency domain):

$$3x_k - 1 = \frac{\beta}{2\pi}\sqrt{\frac{c}{L}}(\frac{L_1}{r_1} + \frac{L_2}{r_2})(\sqrt{1+x_k} - 2\sqrt{1-x_k}) \tag{12}$$

with $x_k = \frac{1}{\pi}\arccos r_k$. We compute numerically this ratio for several configurations.

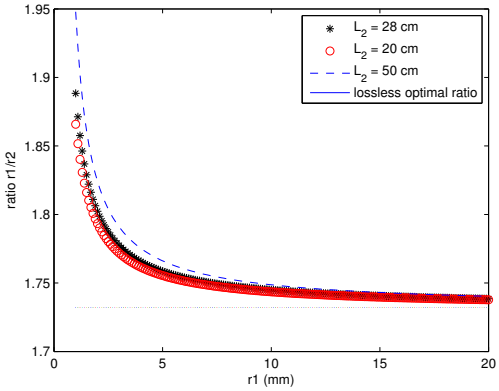

Figure 3: Ratio between radiuses to fulfill the harmonicity condition for the first partials. Both r_1 and lengths vary.

On Figure 3 we see that a good choice for dimensioning the resonator consists in taking a ratio between the low-frequency optimal ratio and the lossless ratio (which is also an optimal high-frequency value). It ensures a good compromise and introduces a slight inharmonicity; which may be responsible for the *ganseo*, a characteristic beating of those flutes. Antaras are believed to be constructed with tools that produce fixed-diameter holes. Then, the length of the small cylinder is adjusted with a cork until the instrument maker reaches the appropriate sound. Figure 4 shows this impact of adjusting the length L_2 on inharmonicity I:

$$I(p) = \frac{f_{res}(p)}{p f_{res}(1)} \tag{13}$$

with $p = 1, 2, 4, 5, 7, 8...$ the partial number.

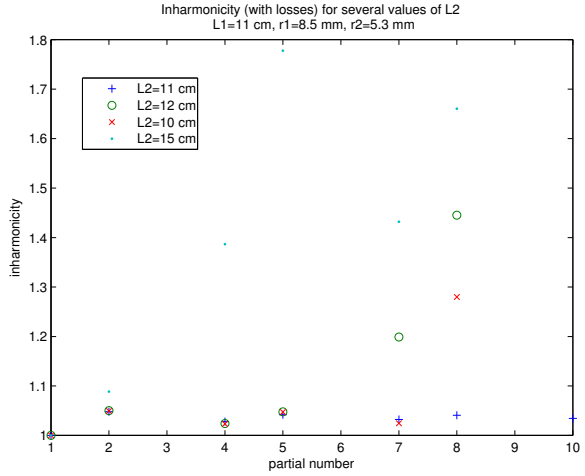

Figure 4: Inharmonicity for several values of L_2

3 Numerical Implementation of the resonator

3.1 Visco-thermal losses

Eq. (14) describes the visco-thermal losses as an analogic filter. We do not take into account propagation because this phenomenon is numerically implemented as a delay line.

$$H_{losses} = e^{-\tilde{\beta}\frac{L}{r}\sqrt{i\omega}}\tilde{\beta} = \frac{\beta}{\sqrt{\pi}} \tag{14}$$

The main difficulty to find an equivalent numerical filter of this transfer function is the nonlinear term $\sqrt{i\omega}$. Current methods [4] consist in designing a static numeric filter that approximates it. Such approximation does not allow the user to modify the parameters of this filter. As we want to keep an explicit dependence of the filter with respect to the physical parameters, we propose a new method to approximate the nonlinear term. We first approximate the exponential:

$$H_{losses} \approx \frac{1 - \frac{\tilde{\beta}}{2}\frac{L}{r}\sqrt{i\omega}}{1 + \frac{\tilde{\beta}}{2}\frac{L}{r}\sqrt{i\omega}} \tag{15}$$

Then, we approximate the term $\sqrt{i\omega}$ with integer powers of $i\omega$. This technique is described in [7] to study fractional derivative. It consists in an approximation of the function $\sqrt{i\omega}$ by piecewise functions of slope 0 and 1 in the log-log domain. This technique has the advantage of being simple and efficient. It approximates the nonlinear term with a stable rational fraction whose coefficients are explicitly known. The order of approximation has to be set initially. We choose the standard frequency range $[20Hz, 2000Hz]$ and a 3-order approximation. Finally, we use the bilinear transform to obtain a numerical filter. It provides an accurate approximation of the analogical filter with a low-order, both in amplitude and phase. We present on Figure 5 the comparison between those filters. It shows that for a range of values of L_1 the approximation remains robust. Other tests with L_2, radius and β have been run and show the same accuracy.

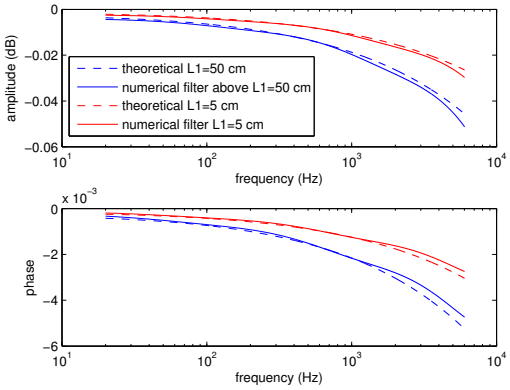

Figure 5: Visco-thermal losses. Comparison between analog and numerical filters.

3.2 Radiation filter

Radiation is described by its impedance defined Eq. (5). From this expression we calculate the corresponding reflection coefficient:

$$H_{rad} = \frac{P^-}{P^+}H_{rad} = \frac{\frac{1}{4}(ka)^2 + i\alpha_i ka - 1}{\frac{1}{4}(ka)^2 + i\alpha_i ka + 1} \tag{16}$$

Then we write it in the numerical domain. A bilinear transform provides a direct way to compute it, but the result is highly unstable. So we write the reflection coefficient in the time domain and then use an approximation of the derivative, such as described in [6]. The result is a 2-order filter stable for a radius $a < 14\ mm$.

$$H_{rad,num} = \frac{(1 + A - B) + (B - 2A)z^{-1} + Az^{-2}}{(A - B - 1) + (B - 2A)z^{-1} + Az^{-2}} \tag{17}$$

with $A = (\frac{aF_s}{2c})^2$ and $B = \frac{aF_s\alpha_i}{c}$.

Similarly to the visco-thermal losses filter, the approximation remains accurate while varying geometrical parameters (see Figure 6).

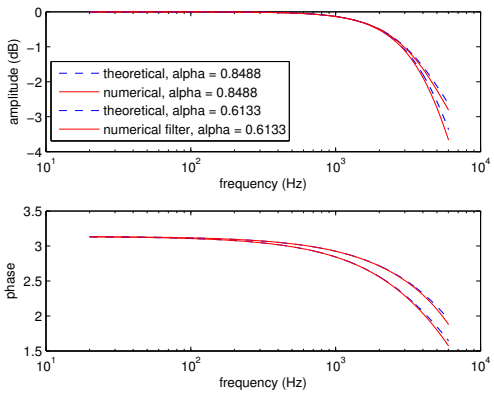

Figure 6: Numerical and analogical reflexion coefficient for several values of α_i

3.3 General scheme for the resonator

Figure 7 shows the different lumped physical elements organized to simulate the complete resonator.

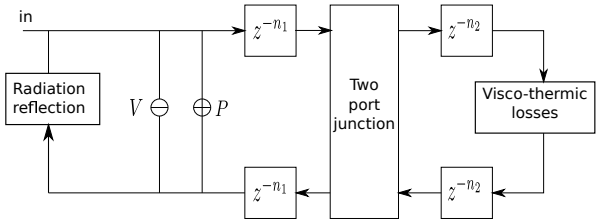

Figure 7: Schematic representation of the synthesis resonator model

The numbers n_1 and n_2 represent the number of samples of the delay line due to the propagation inside the first and second cylinder. Then can be fractional, therefore fractional delay lines are implemented as described in [5]. The two-port junction is implemented according to Eq. (1).

3.4 Synthesis resonator optimization

Exciting the synthesis resonator described above with an impulse as input is used to measure its admittance. A good correspondance between the synthesis resonator and the experimental measurements is observed (see Figure 8). There are though, some differences between them. These differences, regarding both resonant frequencies position and amplitude, come from imperfections of the model or from the slight error between the analogical model and the numerical system.

The synthesis program coefficients explicitly depend on the physical parameters of the flute. Thus we can optimize the synthesis resonator so that it fits a given input admittance. This way, we can build a synthesis resonator as close as possible to a real instrument.

The optimization problem is solved as follow: for an experimental admittance Y_{exp}, we find Y such as it minimizes the cost function defined Eq. (18).

$$C = (|Y_{exp}||Y - Y_{exp}|)^2 \tag{18}$$

The weight factor $|Y_{exp}|$ refines the optimization in the neighborhood of the resonant frequencies.

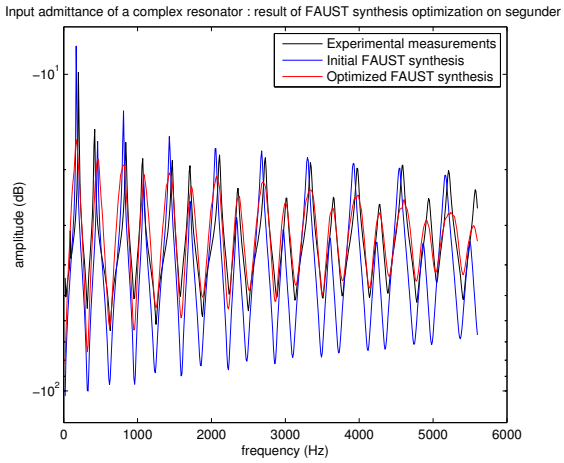

Figure 8: Input admittance amplitude of an antara-like flute. Comparison between measurement and synthesis, before and after the optimization.

The test conducted on a real antara-like flute (cf. Figure 8) shows a very good matching between the recalibration of the synthesis model and the experimental data. The residual error can be explained by an imperfection of the initial acoustic model.

4 Sound synthesis

The model has been implemented in Faust [8], a functional programming language specifically designed for real-time signal processing and synthesis. It is also a practical tool to export the model as a MAX patch, widely used in the community of computer-music composers.

Synthesis program is implemented for two types of antara, the two sections antara, and another type of antara with 3 tubes (see Figure 9). For this last, we simply adapted the model by adding a two-port junction, delay lines and adjustments on the filters. Some presets have been previously defined so that the user has a simple yet complete control on the parameters.

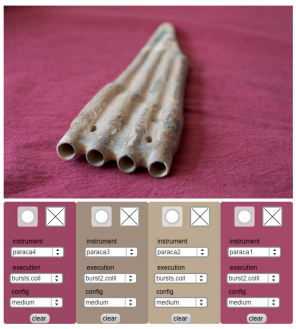

Figure 9: Screenshot of an antara MAX patch synthesis

The variety of sounds we obtain with those synthesizers is wide. It goes from very smooth and aeolian flute sound to dissonant, aggressive and vibrant sound (*sonido rajado*). This shows that the model includes all the elements that explain the production of this particular sound. However, obtaining it requires a very precise setting of the control parameters, especially the excitation variables.

5 Conclusion

We proposed a complete model for the resonator of Andean closed pipes with complex resonators. Resonant frequencies have been analyzed to highlight the influence of geometry on those resonances. Such considerations leads to a better understanding of the elements that need to be considered when building antara-like instruments, capable of producing *sonido rajado*. We have also built a physically based synthesis program entirely controllable by the user. This tool provides a test-bed to study the links between physical parameters and musical aspects as well as a musically friendly interface to be used by computer-music composers.

References

[1] A. Chaigne, J. Kergomard, "Acoustique des instruments de musique", *Belin* (2008)

[2] F. Blanc, P. de La Cuadra, B. Fabre, G. Castillo, C. Vergez, "Acoustics of the Flautas de Chinos", *Proc.*

of 20th Int. Symposium on Music Acoustics Sydney and Katoomba (2010)

[3] P. de La Cuadra, "Input impedance measurements of complex resonator flutes", *https://ccrma.stanford.edu/ pdelac/Antaras/html/*

[4] P. de La Cuadra, "The sound of oscillating air jets", PhD Thesis, Stanford University (2005)

[5] T. Laakso, V. Välimäki, M. Karjalainen, U. Laine, "Splitting the Unit Delay", *IEEE Signal Processing Magazine* (1996)

[6] M-P. Verge, "Aeroacoustics of confined jets, with applications to the physical modeling of recorder-like instruments", Technische Universiteit Eindhoven (1995)

[7] D. Matignon, "Représentations en variables d'état de modèles de guides d'ondes avec dérivation fractionnaire", Université Paris XI Orsay (1994)

[8] FAUST (Functional Audio Stream). *http://faust.grame.fr*